Galectin-1 is essential in tumor angiogenesis and is a target for antiangiogenesis therapy.

Victor L. J. L. Thijssen, Ruben Postel, Ricardo J. M. G. E. Brandwijk, Ruud P. M. Dings, Irina Nesmelova, Sietske Satijn, Nicole Verhofstad, Yusaku Nakabeppu, Linda G. Baum, Jeroen Bakkers, et al.

Classification: Biological Sciences; Medical Sciences

Galectin-1 is essential in tumor angiogenesis and is a target for anti-angiogenesis therapy.

Victor LJL Thijssen[a], Ruben Postel[b], Ricardo JMGE Brandwijk[a], Ruud PM Dings[c], Irina Nesmelova[c], Sietske Satijn[a], Nicole Verhofstad[a], Yusaku Nakabeppu[d], Linda G Baum[e], Jeroen Bakkers[b], Kevin H Mayo[c], Françoise Poirier[f], Arjan W Griffioen[a]

a. Angiogenesis Laboratory, Research Institute for Growth and Development (GROW), Dept of Pathology, University Maastricht, Maastricht, The Netherlands.
b. Netherlands Institute for Developmental Biology and Interuniversity Cardiology Institute of the Netherlands, Hubrecht Laboratory, Utrecht, The Netherlands.
c. Dept of Biochemistry, Molecular Biology & Biophysics, University of Minnesota, Minneapolis, USA.
d. Division of Neurofunctional Genomics, Dept of Immunobiology and Neuroscience, Medical Institute of Bioregulation, Kyushu University, Fukuoka, Japan.
e. Dept of Pathology and Laboratory Medicine, University of California, School of Medicine, Los Angeles, USA.
f. Institut Jacques Monod, UMR CNRS 7592, Univ. P6 and P7, Paris, France.

Corresponding author: Arjan W. Griffioen, PhD. Dept of Pathology, Angiogenesis Laboratory, Maastricht University & University Hospital Maastricht, PO Box 5800, 6202 AZ Maastricht, The Netherlands, e-mail: aw.griffioen@path.unimaas.nl, T +31 43 3874630, F +31 43 3876613

Manucript information: 23 text pages, 4 figures

Words in abstract: 120

Number of characters (text): 35657

Number of characters (figures): 10440

Abstract

We describe that galectin-1 is a receptor for the angiogenesis inhibitor anginex and that the protein is crucial for tumor angiogenesis. Galectin-1 is overexpressed in endothelial cells of different human tumors. Expression knockdown in cultured endothelial cells inhibits cell proliferation and migration. The importance of galectin-1 in angiogenesis is illustrated in the zebrafish model, where expression knockdown results in impaired vascular guidance and growth of dysfunctional vessels. The role of galectin-1 in tumor angiogenesis is demonstrated in galectin-1 null mice, in which tumor growth is markedly impaired due to insufficient tumor angiogenesis. Furthermore, tumor growth in galectin-1 null mice no longer responds to anti-angiogenesis treatment by anginex. Thus, galectin-1 regulates tumor angiogenesis and is a target for angiostatic cancer therapy.

Introduction

An adequate vasculature is a prerequisite for tumors to grow, and the need for neovessel formation (or angiogenesis) provides a target for treatment of cancer (1). Endothelial cells (EC) that line the tumor vasculature are particularly suitable target cells for therapeutic approaches since they are easily accessible to agents delivered via the blood (2). However, to affect only tumor vasculature, specific targets on angiogenically active EC are essential. To date, only a few targets of tumor vasculature have been identified (3).

We recently developed the specific angiostatic peptide anginex that inhibits tumor growth through specific inhibition of angiogenesis (4-6). Although a broad profile of activities of anginex is known, such as prevention of EC adhesion and induction of apoptosis, the molecular target on tumor EC was never identified. In a receptor finding study using a yeast two-hybrid screening approach, we identified galectin-1 as a target protein of anginex.

Galectin-1 belongs to a family of carbohydrate binding proteins that share a conserved carbohydrate recognition domain (CRD) of approximately 130 amino acids (7-9). Over a dozen mammalian galectins have been described (10, 11) and members of this family are expressed in a wide range of species, suggesting an important role for galectins in basic cellular mechanisms. Galectins can be secreted, and depending on the cell type or state of differentiation, they have been found in the nucleus, in the cytoplasm, or in the extracellular matrix. It has been proposed that galectin-1 mediates cell adhesion and migration (12), and is involved in several processes including proliferation (13), apoptosis (14), and even mRNA splicing (15). The role of galectin-1 in EC function or in vascular biology has not been extensively studied.

Here, we describe the function of galectin-1 in the angiogenesis. We provide direct functional evidence that galectin-1 is required for tumor angiogenesis and for outgrowth of tumors. Furthermore, we show that galectin-1 is the target for the potent angiogenesis inhibitor anginex, thus establishing galectin-1 as an important target for anti-cancer therapy.

Results

Galectin-1 binds the angiostatic peptide anginex.

The goal of the present study was to identify the receptor of anginex, an angiogenesis inhibitor which has previously been shown to specifically target tumor endothelial cells (EC) (5). Immunohistochemistry revealed vesicular uptake of anginex by EC within 2 hours **(Fig. 1A)**. Electron microscopy showed anginex located at the membrane of intracellular vesicles, suggesting receptor-mediated uptake **(Fig. 1B)**. To identify this receptor, yeast two-hybrid (Y2H) analysis was performed. To that end, the recently described artificial anginex gene (16) was cloned in frame with the GAL-4 DNA binding domain of the Y2H bait vector pGBDT7, which was confirmed by Western blotting **(not shown)**. Multiple screens against cDNA libraries of activated EC identified galectin-1 (gal-1) as the receptor for anginex **(Suppl. Table 1/Suppl. Fig. 1)** which was independently confirmed using three approaches. i) Double staining of anginex treated EC showed co-localization of anginex and gal-1. ii) Analysis of NMR spectra revealed chemical shift changes of certain resonances from gal-1 upon addition of anginex, indicative of a specific molecular interaction. iii) Plasmon resonance spectroscopy (BIAcore analysis) was used to further define the kinetics and stoichiometry of the interaction. Analysis of the binding kinetics revealed a 1:1 Langmuir association with a rate constant (k_a) of ~6.5×10^3 Ms^{-1}, while the dissociation kinetics followed a biphasic pattern with dissociation rate constants of 4.2×10^{-2} s^{-1} and 5.9×10^{-4} s^{-1}, respectively**.** These data suggest that dimerized anginex binds to gal-1 and that subsequently the two anginex molecules dissociate as monomers with a K_d of 6.4 μM for dissociation of first anginex molecule and a K_d of 90 nM for the second molecule. This result is supported by mass spectrometry which displayed a major peak with a mass of 22.8 kD (gal-1 monomer (14.7 kD) + anginex dimer (8 kD) **(not shown)**. The data above show that gal-1 and anginex interact, suggestive of gal-1 serving as receptor for anginex.

Galectin-1 is overexpressed in tumor EC; a crucial role in EC proliferation and migration.

To determine the role of gal-1 in tumor EC biology, we first analyzed gal-1 expression in human tumor blood vessels by immunohistochemistry. While gal-1 is only weakly expressed in EC of normal tissue **(colon is shown: Figure 1C, left panels),** a strong expression was found in EC of human colon carcinoma **(Figure 1C, middle panels)** and breast carcinoma **(not shown)**, especially in EC that stained positive for the proliferation marker Ki67. Similar results were observed for a sarcoma type of tumor (Ewing sarcoma) in which the gal-1 staining was almost exclusively observed in vessels **(Figure 1C, right panels)**. These data demonstrate that the amount of gal-1 protein is upregulated in angiogenically active EC. Indeed, growth factor activation of freshly isolated human umbilical vein EC resulted in a significant increase in gal-1 mRNA expression and a concomitant >10-fold induction of gal-1 protein expression **(Figure 1D)**. Furthermore, treatment of activated EC with a gal-1 specific antisense oligodeoxynucleotide (ODN) resulted in inhibition of EC proliferation, while a random ODN had no effect **(Figure 1E)**. Next to EC proliferation, EC migration was also inhibited by treatment with either the gal-1 specific ODN **(Figure 1F)** or the rabbit polyclonal anti-gal-1 antibody **(Figure 1G).** These data strongly suggest a role for gal-1 in EC biology.

Galectin-1 is required for coordinated angiogenesis *in vivo*.

The role of gal-1 in angiogenesis *in vivo* was first studied in the chick chorioallantoic membrane (CAM). Treatment of the CAM with a rabbit polyclonal anti-gal-1 antibody induced a significant inhibition of microvessel density, similar as previously published for anginex (4-5) albeit less pronounced. Interestingly, treatment caused tortuous and irregular growth of the vessels, suggesting a defect in vascular guidance **(Suppl. Fig. 2)**. For further insight in the role of gal-1 during angiogenesis *in vivo*, we used the *Tg(fli1:egfp)*^{y1} zebrafish model. In this model, EC are marked by expression of green fluorescent protein (GFP) (17). Recently, 3 prototype galectins

were described in zebrafish (Lgals1-L1/L2/L3) of which Lgals1-L2 was found to preferentially bind N-acetyllactosamine, similar to human gal-1 (18). Since *Lgals1-L1* is not expressed during embryogenesis (18) we only studied the role of the other two prototype galectins in vascular development. Whole mount RNA *in situ* hybridization at 48 hours post-fertilization revealed specific expression of *Lgals1-L2* in the eyes around the lens and in the ventricular zone in the head **(Figure 2A).** *Lgals1-L3* expression was broader and largely overlapped with that of *Lgals1-L2* **(Figure 2B)**. Furthermore, cross sections at the level of the midbrain showed co-localization of both *Lgals1-L2/-L3* and the EC specific marker *VE-cadherin* in the retinal vessels **(Figures 2C-E)** and in the blood vessels in the brain **(not shown)**.

To determine the function of *Lgals1-L2* and *-L3* on vascular development, morpholino-modified antisense oligonucleotides (MOs) were designed to specifically target either the translation start site (ATG-MO) or the splice donor site (splice-MO). We verified that injection of each splice-MO successfully interfered with the splicing of the respective transcripts **(not shown)**. Injection of either *Lgals1-L2* or *-L3* ATG-MO induced hemorrhages in the head and in/behind the eyes of the embryos at 2.5 days post fertilization, as detected with a sensitive o-Dianisidine blood staining. Co-injection of both *Lgals1-L2* and *-L3* MOs resulted in even more severe hemorrhages **(Figures 3A-D)**. Similar results were observed with the splice-MOs **(not shown)**. Confocal scanning laser microscopy in the ventricular zone of *Tg(fli1:egfp)*^{y1} zebrafish revealed vascular defects, at the location of the hemorrhages, after co-injection of *Lgals1-L2* and *-L3* ATG MO. Compared to untreated zebrafish **(Figure 3F)**, abnormal sprouting and misguidance of vessels clearly appeared in the mid-cerebral area of the *Lgals1-L2* and *-L3* ATG MO treated animals **(Figures 3E-H)**. Vascular network formation of the middle cerebral-, dorsal longitudinal-, mesencephalic- and anterior cerebral veins was also distorted by both MOs, and most severely in the double knockdown **(Figure 3G)**. The same defects were observed upon co-injection of both splice MOs, indicating specificity of the knockdown defects **(Figure 3H)**, while single injection

of each splice MO revealed weaker defects **(not shown)**. Similar to those in the ventricular zone, retinal vessels showed abnormal sprouting and growth in the regions where hemorrhages occurred **(not shown)**. Together with observations from the CAM, results in zebrafish indicate that gal-1 is important *in vivo* for coordinated vessel outgrowth and vascular network formation.

Galectin-1 facilitates tumor progression through angiogenesis.

The presented results urged us to study the role of gal-1 by analyzing tumor angiogenesis in the gal-1 null mice (19). To compare tumor growth in the presence or absence of gal-1, wild type (gal-$1^{+/+}$) and null (gal-$1^{-/-}$) mutant 129P3/J mice were subcutaneously injected with syngeneic murine F9 teratocarcinoma cells. Three days after injection, a small palpable tumor developed in all mice, suggesting that tumor initiation and initial growth is not dependent on gal-1. However, subsequent tumor growth was significantly abrogated in the gal-$1^{-/-}$ mice compared to the wild-type animals. Fifteen days after injection, the tumor volumes in the gal-$1^{-/-}$ mice were approximately 4-fold smaller compared to those in the gal-$1^{+/+}$ mice **(Figure 4A)**. As expected, immunohistochemical analysis showed high expression of gal-1 in the EC of tumor vessels in the wild-type animals and no expression in the null mice **(Figure 4B)**. Quantification of microvessel density revealed a significant lower amount of blood vessels in null mice compared to wild-type mice **(Figure 4C)**. In addition, parameters of vessel architecture were decreased **(Suppl. Table 2)**. Since gal-1 has been shown to mediate apoptosis in activated T cells, which could contribute positively to tumor growth (20), we also quantified the amount of peripheral blood leukocytes, and the presence of $CD45^+$ and $CD8^+$ cells in the tumors. There was no significant difference in these parameters between gal-$1^{+/+}$ and gal-$1^{-/-}$ animals **(Suppl. Fig. 3)** which strongly suggests that, in this particular model, impaired tumor progression in gal-1 null mice largely results from decreased angiogenesis.

Galectin-1 is a target protein for angiostatic therapy.

Because gal-1 was initially identified as a receptor for the angiostatic peptide anginex, we also analyzed the effect of anginex treatment in wild type and gal-1 null mice. In wild-type animals, anginex significantly inhibited tumor growth by approximately 70% **(Figure 4D)** and vessel density by approximately 55% **(Figure 4E)**, which is comparable with previous observations for anginex in other tumor models (5, 21). In gal-$1^{-/-}$ mice, treatment with anginex had no effect on tumor growth **(Figure 4F).** In addition, anginex treatment did not significantly affect the number of infiltrating $CD45^{+}$ or $CD8^{+}$ cells in the tumors of both the wild type and null mice **(Suppl. Fig. 4)**. These data demonstrate that gal-1 mediates the angiostatic activity of anginex and that gal-1 can serve as a target for angiostatic therapy.

Discussion

The current study is the first to demonstrate that gal-1 is important in tumor angiogenesis and that targeting of gal-1 can be an efficient angiostatic therapeutic strategy. Previous studies have shown that gal-1 is key in two mainstays of cancer. Firstly, gal-1 supports metastasis formation, because it facilitates interactions between tumor cells and endothelial cells (EC) (22, 23). Secondly, it protects the tumor against immunity since it can induce apoptosis in tumor infiltrating cytotoxic leukocytes (14, 20). This study now reports a critical role in angiogenesis, a third important pillar in tumor growth. Our results reveal a direct role of gal-1 in EC biology. We found a direct involvement of gal-1 in EC proliferation and migration *in vitro* and in tumor angiogenesis *in vivo*. While the angiogenesis-independent onset of F9 tumor growth was similar in gal-1 null and wild type mice, the angiogenesis dependent outgrowth of tumors was severely hampered in the null mice. The low microvessel density in the null mice led us to conclude that the abrogated tumor growth is caused by inefficient angiogenesis. It has been shown that gal-1 null mice have subtle neuronal abnormalities that become apparant upon challenge (24, 25). In line with this, the effect on angiogenesis also becomes apparent by challenging the mice with a growing tumor. This corroborates with our observations in the CAM and the zebrafish, in which acute interference with gal-1 function also results in aberrant angiogenesis. Obviously, the presence of gal-1 is required for a proper response to an acute stress or pressure on EC biology and angiogenesis. It remains to be investigated whether vascular development in the null mice is indeed normal, or that subtle vascular defects do exist.

We also observed that intervening with gal-1 function results in irregular patterning of the vasculature. The abnormal vessel architecture in the CAM, the zebrafish model, and in knockout mice tumors, suggest that gal-1 is involved in vascular network formation. Recent studies have shown that the development of both vascular and neuronal networks is regulated by the same receptor/ligand pairs, i.e. Robos/Slits, Ephrins/Eph receptors, Neuropilins/Semaphorins, and

Netrins/Unc5B (26, 27). Interestingly, for gal-1 a role in neuronal pathfinding has already been identified (28). Furthermore, gal-1 null mice show neuronal abnormalities in adulthood (25). Together with the role of gal-1 in angiogenesis described here, these data strongly suggest that gal-1, as well as other members of the galectin family (galectin-3 (29, 30)) are also involved in both neuronal and vascular development.

It has been proposed that galectins can serve as molecular targets for cancer therapy (20, 31-33). Interestingly, we identified gal-1 as a receptor for the angiostatic peptide anginex. Anginex has been shown to inhibit tumor growth by inhibition of tumor angiogenesis (4-6). A previous study reported that transport to the tumor vasculature is facilitated by fibronectin (34). Our results now show that for the angiostatic activity on EC, galectin-1 is required. Anginex treatment in gal-1 null mice did not result in further inhibition of the already hampered tumor growth, while wild type mice responded as reported previously (5, 6). This indicates that gal-1 is essential for the activity of anginex and that gal-1 can indeed serve as a target for angiostatic cancer therapy. We also observed high expression of gal-1 in EC in mouse tumors as well as in human colon and breast carcinomas. There are other reports on the expression of gal-1 in tumor stroma, mainly in studies comparing the expression between normal and cancerous tissues (reviewed by (33)). Elevated stromal expression of gal-1 has been reported in several cancers including cancer of the ovaries (35), breast (36), prostate (37), and colon (38). These results suggest that the increased expression in tumors makes the protein an excellent target for diagnostic or therapeutic purposes.

It is attractive to speculate that, since gal-1 is crucial in several prerequisites for unlimited tumor growth, gal-1 targeting compounds may have multimodal activities. Interfering with gal-1 function could (i) prevent metastasis formation through inhibition of gal-1 facilitated tumor cell-EC interactions (22, 23), (ii) abrogate tumor escape from immunity through blockade of gal-1

induced apoptosis in activated T lymphocytes (14, 20), and (iii) prevent the execution of tumor angiogenesis (this study). This makes gal-1 an excellent target for cancer therapy.

Materials and Methods

Cell cultures

Human umbilical vein EC (HUVEC) and the human microvascular EC line HMEC were cultured as described elsewhere (5). F9 teratocarcinoma cells (kind gift from Dr. H. Weich) were cultured in RPMI-1640 supplemented with 10% fetal bovine serum, 1% glutamin, 50 U/ml penicillin, and 50 ng/ml streptomycin.

Mouse tumor model

A total of 14 adult 129P3/J gal-$1^{-/-}$ mutant mice (19) and 17 matched 129P3/J gal-$1^{+/+}$ (wild type) mice were used in this study. On day 1, animals were injected s.c. with $3x10^6$ syngeneic F9 teratocarcinoma cells. On day 7, anginex treatment (10 mg/kg/day) was started in 7 wild type and 9 mutant mice by daily i.p. injections. Tumor volume and mouse weight were measured daily throughout the experiment. Animals were given water and standard chow ad libitum, and they were kept on a 12-hour light/dark cycle. All experiments were approved by the local ethical review committee.

Knockdown of galectin-1 expression *in vitro*

Knockdown of gal-1 expression *in vitro* was obtained using a gal-1 specific antisense oligodeoxynucleotide (hgal1 ODN: GTCACCGTCAGCTGCCATGT). As control, a random nonspecific antisense oligodeoxynucleotide (control ODN: TCCCTAGTGACTCTTCCC) was used. ODNs were renewed every other day.

FACS analysis

FACS analysis of gal-1 protein expression was performed on ethanol fixed HUVEC. Cells were washed in 0.1% BSA/0.01% sodium azide/PBS, incubated on ice with polyclonal rabbit anti-galectin antibody (39), and washed with PBS. Next, the cells were incubated with FITC-labeled polyclonal goat anti-rabbit Ig antibody (Dako) and washed with PBS. Five thousand events were acquired for each sample on a FACSCalibur flow cytometer (Beckton Dickinson). All experiments were performed in triplicate.

Migration, proliferation, and CAM assay

Migration, proliferation, and CAM assays were performed as described elsewhere (16). Within each proliferation experiment, treatments were done in triplicate and all proliferation and migration experiments were performed at least three times. For the CAM, two independent experiments were performed (overall n = 13 / treatment group).

Real-time PCR

Total RNA isolation, subsequent cDNA synthesis, and real-time PCR were performed as described previously (40) with primers targeted against human gal-1 (Forward: TGCAACAGCAAGGACGGC; Reverse: CACCTCTGCAACACTTCCA). Primers were purchased from Eurogentec and experiments were performed in triplicate.

Immunohistochemistry

Immunohistochemical staining of anginex uptake was performed on HUVEC cytospins. Cells were acetone fixed and air dried. Following incubation in 1% paraformaldehyde cells were incubated in fetal calf serum after which mouse 2D10 monoclonal anti-anginex antibody (5) was applied in 0.05% Triton X100/PBS. Following incubation with Texas Red labeled goat-anti-

mouse Ig antibody, the cells were washed with PBS and mounted in Immumount (Shandon Inc.) supplemented with 1 μg/ml 4',6-diamidino-2-phenylindole (DAPI; Molecular Probes). In the negative control, incubation with the first antibody was omitted.

Doublestaining for Ki67 and CD31/34 on paraffin-embedded tissue sections was performed as previously described (41). Tissues from normal colon, colon carcinoma, and Ewing sarcoma were obtained from the stocks of the Department of Pathology, University Hospital Maastricht. For gal-1 staining, paraffin-embedded tissue sections were dewaxed and endogenous peroxidase activity was blocked with 0.3% H_2O_2 in methanol. Next, the slides were microwave pretreated in citric acid. After blocking with 1% BSA/PBS primary antibody was applied in 0.5%BSA/PBS. Next, biotin-labeled secondary antibody was applied and staining was performed with the StreptABComplex/HRP kit (Dako) according the suppliers protocol. The tissue sections were counterstained with haematoxilin (Merck), dehydrated and mounted in Entellan (Merck). The same protocol was used for EC staining with the EC specific antibody 9F1 (42). Staining for CD45+ and CD8+ cells was performed on frozen tissue sections which were fixed in acetone and air dried. Endogenous peroxidase activity was blocked with 0.3% hydrogen peroxidase/PBS and aspecific binding was blocked with 20% FCS/0.1% Tween20/PBS. Next, the primary antibody (MP33 rat anti-mouse CD45 or 53.6.27 rat anti-mouse CD8) was applied, followed by incubation with biotin labeled secondary antibody. Staining was visualized using the Vectastain ABC kit (Vector Laboratories) and subsequently, sections were counterstained with haematoxylin, dehydrated, and mounted with Entellan. Within each section, the number of positive cells was scored at 4 different locations in a blinded fashion by two different observers. Fluorescent staining of CD31 in murine tumors and subsequent scoring of vessel characteristics was performed as described before (6).

Zebrafish experiments

For *in vivo* experiments, the previously described *Tg(fli1:egfp)*^{y1} zebrafish was used (17). Knock-down of *Lgals1-L2* and *-L3* expression was achieved by injection of specific morpholino-modified antisense oligonucleotides (MOs; Genetools) into 1-cell stage embryos (43). The following MOs were used: *Lgals1-L2* ATG-MO, 5'-GTATAAGCACACCGGCCATTTTGAC-3'; *Lgals1-L3* ATG-MO, 5'-AAGATCCCAGGCTAAGGACGTCATT-3'; *Lgals1 L2* splice-MO, 5'-TTGTAATATACTCACGGCCATTTTG-3'; *Lgals1 L3* splice-MO, 5'-ATGTCTGTACTCACGCATCACAGCC-3'. Before 24 hours post-fertilization (hpf), 1-Phenyl-2-thiourea (PTU, 0.002%) was added to prevent pigment development. For imaging, dechorionated embryos were anesthetized with 0.003% tricaine methanesulfonate and mounted in 2% low melting agarose. Confocal scanning microscopy was performed using a Leica TCS NT. For whole mount blood staining, dechorionated and PTU treated embryos were incubated in 40% EtOH, 0.01M NaAc pH5.2, 2.0% H_2O_2, in the presence of 0.8 mg/ml o-dianisidine. Following rehydration in a graded series of EtOH/PBST the embryos were stored in 50% glycerol at 4°C. Whole mount *in situ* hybridization on zebrafish embryos was carried out as previously described (44). For *VE-cadherin* riboprobe synthesis we used the previously published plasmid (45). For *Lgals1-L2* antisense probe synthesis RZPD clone IMAGp998D0710947Q3 (in pSPORT1) was linearized with *Bam*HI and transcribed with T7 RNA polymerase. Zebrafish *Lgals1-L3* was cloned from RZPD clone IMAGp998J1712051Q3 into pBluescript KS giving rise to *lgal1-L3*/pBs. For *lgal1-L3* antisense probe synthesis, plasmid *lgal1-L3*/pBs was linearized with Acc65I and transcribed with T7 RNA polymerase. For sectioning, the embryos were embedded in Technovit 8100 (Heraeus Kulzer, Wehrheim Germany). Seven µM thick sections were cut and counterstained with neutral red dye.

Statistics

All data are shown as mean with standard error except where indicated otherwise. Data from i*n vitro* proliferation, real-time PCR, CAM assay, FACS analysis, and CD45/CD8 scores were analyzed using the Mann-Whitney U test. Tumor growth curves and migration assay data were analyzed using 2-way ANOVA. The Student's t-test was used to analyze the vascular parameters. All values are two-sided and P-values<0.05 were considered statistically significant. Two-way ANOVA was performed in Graphpad Prism 3.0 (Graphpad Software Inc.). All other statistical computations were performed in SPSS 10.0.5. (SPSS Inc.).

Acknowledgements

The authors are grateful for excellent assistance of S Chocron for *in situ* hybridizations and sectioning, Drs. P Frederik and D van der Schaft for the EM experiments, Dr. H Weich for providing the F9 teratocarcinoma cells, Dr. A Hamann for providing the 9F1 antibody, Drs. W Roeffen and M Roestenberg for their help with the BIAcore experiments, Drs. C Baeten and F Hillen for CD8/CD45 scoring, and Drs. S Ekker, Dr. S Schulte-Merker and Dr. D Stainier for providing reagents. We thank M Pang for the production of recombinant gal-1 and Dr. W Buurman for critical reading of the manuscript. This research was supported in part by a grant from the National Institutes of Health USA (CA 096090) to KHM. AG was supported by a grant from the Technology Foundation STW, applied science division of NWO and the technology program of the Ministry of Economic Affairs. FP was a recipient of grants from GEFLUC, ARC and LN CC. LGB was a recipient of a grant from the Cancer Research Institute.

References

1. Folkman, J. (1972) *Ann Surg* **175,** 409-16.
2. Griffioen, A. W. & Molema, G. (2000) *Pharmacol Rev* **52,** 237-68.
3. van Beijnum, J. R. & Griffioen, A. W. (2005) *Biochim Biophys Acta* **1755,** 121-34.
4. Griffioen, A. W., van der Schaft, D. W., Barendsz-Janson, A. F., Cox, A., Struijker Boudier, H. A., Hillen, H. F. & Mayo, K. H. (2001) *Biochem J* **354,** 233-42.
5. van der Schaft, D. W., Dings, R. P., de Lussanet, Q. G., van Eijk, L. I., Nap, A. W., Beets-Tan, R. G., Bouma-Ter Steege, J. C., Wagstaff, J., Mayo, K. H. & Griffioen, A. W. (2002) *Faseb J* **16,** 1991-3.
6. Dings, R. P., van der Schaft, D. W., Hargittai, B., Haseman, J., Griffioen, A. W. & Mayo, K. H. (2003) *Cancer Lett* **194,** 55-66.
7. Drickamer, K. (1988) *J Biol Chem* **263,** 9557-60.
8. Hirabayashi, J. & Kasai, K. (1993) *Glycobiology* **3,** 297-304.
9. Barondes, S. H., Castronovo, V., Cooper, D. N., Cummings, R. D., Drickamer, K., Feizi, T., Gitt, M. A., Hirabayashi, J., Hughes, C., Kasai, K. & et al. (1994) *Cell* **76,** 597-8.
10. Cooper, D. N. (2002) *Biochim Biophys Acta* **1572,** 209-31.
11. Houzelstein, D., Goncalves, I. R., Fadden, A. J., Sidhu, S. S., Cooper, D. N., Drickamer, K., Leffler, H. & Poirier, F. (2004) *Mol Biol Evol* **21,** 1177-87.
12. Hughes, R. C. (2001) *Biochimie* **83,** 667-76.
13. Scott, K. & Weinberg, C. (2004) *Glycoconj J* **19,** 467-77.
14. Perillo, N. L., Pace, K. E., Seilhamer, J. J. & Baum, L. G. (1995) *Nature* **378,** 736-9.
15. Park, J. W., Voss, P. G., Grabski, S., Wang, J. L. & Patterson, R. J. (2001) *Nucleic Acids Res* **29,** 3595-602.
16. Brandwijk, R. J., Nesmelova, I., Dings, R. P., Mayo, K. H., Thijssen, V. L. & Griffioen, A. W. (2005) *Biochem Biophys Res Commun* **333,** 1261-1268.

17. Lawson, N. D. & Weinstein, B. M. (2002) *Dev Biol* **248,** 307-18.

18. Ahmed, H., Du, S. J., O'Leary, N. & Vasta, G. R. (2004) *Glycobiology* **14,** 219-32.

19. Poirier, F. & Robertson, E. J. (1993) *Development* **119,** 1229-36.

20. Rubinstein, N., Alvarez, M., Zwirner, N. W., Toscano, M. A., Ilarregui, J. M., Bravo, A., Mordoh, J., Fainboim, L., Podhajcer, O. L. & Rabinovich, G. A. (2004) *Cancer Cell* **5,** 241-51.

21. Dings, R. P., Yokoyama, Y., Ramakrishnan, S., Griffioen, A. W. & Mayo, K. H. (2003) *Cancer Res* **63,** 382-5.

22. Lotan, R., Belloni, P. N., Tressler, R. J., Lotan, D., Xu, X. C. & Nicolson, G. L. (1994) *Glycoconj J* **11,** 462-8.

23. Clausse, N., van den Brule, F., Waltregny, D., Garnier, F. & Castronovo, V. (1999) *Angiogenesis* **3,** 317-25.

24. McGraw, J., McPhail, L. T., Oschipok, L. W., Horie, H., Poirier, F., Steeves, J. D., Ramer, M. S. & Tetzlaff, W. (2004) *Eur J Neurosci* **20,** 2872-80.

25. McGraw, J., Gaudet, A. D., Oschipok, L. W., Steeves, J. D., Poirier, F., Tetzlaff, W. & Ramer, M. S. (2005) *Pain* **114,** 7-18.

26. Klagsbrun, M. & Eichmann, A. (2005) *Cytokine Growth Factor Rev* **16,** 535-48.

27. Weinstein, B. M. (2005) *Cell* **120,** 299-302.

28. Puche, A. C., Poirier, F., Hair, M., Bartlett, P. F. & Key, B. (1996) *Dev Biol* **179,** 274-87.

29. Nangia-Makker, P., Honjo, Y., Sarvis, R., Akahani, S., Hogan, V., Pienta, K. J. & Raz, A. (2000) *Am J Pathol* **156,** 899-909.

30. Kuklinski, S., Vladimirova, V., Waha, A., Kamata, H., Pesheva, P. & Probstmeier, R. (2003) *J Neurochem* **87,** 1112-24.

31. Zou, J., Glinsky, V. V., Landon, L. A., Matthews, L. & Deutscher, S. L. (2005) *Carcinogenesis* **26,** 309-18.

32. Liu, F. T. & Rabinovich, G. A. (2005) *Nat Rev Cancer* **5,** 29-41.

33. van den Brule, F., Califice, S. & Castronovo, V. (2004) *Glycoconj J* **19,** 537-42.

34. Akerman, M. E., Pilch, J., Peters, D. & Ruoslahti, E. (2005) *Proc Natl Acad Sci U S A* **102,** 2040-5.

35. Allen, H. J., Sucato, D., Woynarowska, B., Gottstine, S., Sharma, A. & Bernacki, R. J. (1990) *J Cell Biochem* **43,** 43-57.

36. Gabius, H. J., Brehler, R., Schauer, A. & Cramer, F. (1986) *Virchows Arch B Cell Pathol Incl Mol Pathol* **52,** 107-15.

37. van den Brule, F. A., Waltregny, D. & Castronovo, V. (2001) *J Pathol* **193,** 80-7.

38. Lotan, R., Matsushita, Y., Ohannesian, D., Carralero, D., Ota, D. M., Cleary, K. R., Nicolson, G. L. & Irimura, T. (1991) *Carbohydr Res* **213,** 47-57.

39. Pace, K. E., Hahn, H. P. & Baum, L. G. (2003) *Methods Enzymol* **363,** 499-518.

40. Thijssen, V. L., Brandwijk, R. J., Dings, R. P. & Griffioen, A. W. (2004) *Exp Cell Res* **299,** 286-93.

41. Lussanet, Q. G., Backes, W. H., Griffioen, A. W., Padhani, A. R., Baeten, C. I., van Baardwijk, A., Lambin, P., Beets, G. L., van Engelshoven, J. M. & Beets-Tan, R. G. (2005) *Int J Radiat Oncol Biol Phys*.

42. Harder, R., Uhlig, H., Kashan, A., Schutt, B., Duijvestijn, A., Butcher, E. C., Thiele, H. G. & Hamann, A. (1991) *Exp Cell Res* **197,** 259-67.

43. Nasevicius, A., Larson, J. & Ekker, S. C. (2000) *Yeast* **17,** 294-301.

44. Hammerschmidt, M., Pelegri, F., Mullins, M. C., Kane, D. A., Brand, M., van Eeden, F. J., Furutani-Seiki, M., Granato, M., Haffter, P., Heisenberg, C. P., Jiang, Y. J., Kelsh, R. N., Odenthal, J., Warga, R. M. & Nusslein-Volhard, C. (1996) *Development* **123,** 143-51.

45. Larson, J. D., Wadman, S. A., Chen, E., Kerley, L., Clark, K. J., Eide, M., Lippert, S., Nasevicius, A., Ekker, S. C., Hackett, P. B. & Essner, J. J. (2004) *Dev Dyn* **231,** 204-13.

46. Isogai, S., Horiguchi, M. & Weinstein, B. M. (2001) *Dev Biol* **230,** 278-301.

Figure legends

Figure 1. Galectin-1 binds to anginex and galectin-1 expression is enhanced in activated EC and tumor EC; role in EC function.

(A) Immunohistochemical detection of anginex treated HUVEC using mouse monoclonal 2D10 anti-anginex antibody (red staining) in a time-lapse experiment. Nuclei are counterstained with DAPI (blue staining). Anginex appears in vesicular structures (arrowheads). In the control, the primary antibody was omitted. Bar in the left panel represents 10 μm. (**B)** Electron microscopy of an immunogold labeling of anginex demonstrating the accumulation of anginex in HUVEC. Inset: Detail showing the membrane localization of anginex (arrowheads). Magnification: 80,500x. **(C)** Gal-1 is overexpressed in EC of human colon carcinoma and Ewing sarcoma as compared to normal human colon. The top panels show a double staining for the EC (CD31/34, blue) and the proliferation marker Ki67 (brown/black). The lower panels show staining of a consecutive section for gal-1 (brown) with hematoxylin as counterstain (blue). The arrows indicate blood vessels. Arrowheads point towards individual proliferating EC. The insets show a detail of gal-1 staining in EC (arrow). **(D)** Gal-1 mRNA (qPCR; n=5) and protein (FACS; n=4) expression are upregulated in activated HUVEC. Expression was determined in cells immediately following isolation from the umbilical vein (native) and after culturing the cells for three additional days in medium containing 20% human serum (active). *$p<0.05$. vs. native. **(E)** Knockdown of gal-1 expression with ODN results in a concentration dependent inhibition of EC proliferation (n=4); *$p<0.05$ vs. control; #$p<0.05$ vs. control ODN. **(F)** Treatment with 1 μM or 5 μM gal-1 ODN results in a significant inhibition of EC migration (n=4); #$p<0.005$ vs. blank; *$p<0.05$ vs. blank. **(G)** Treatment with a gal-1 antibody results in a significant inhibition of EC migration (n=3); #$p<0.005$ vs. PBS; *$p<0.01$ vs. PBS.

Figure 2. Expression of zebrafish *Lgals-1 L2* and *Lgals-1 L3*.

Whole mount *in situ* hybridization on 48h zebrafish embryos. **(A)** *Lgals-1 L2* is strongly expressed in the eyes around the lens (arrow) and in the ventricular zone in the head (arrowheads). **(B)** *Lgals-1 L3* expression is less restricted but does overlap with *L2* expression around the lens (arrow) and in the ventricular zone (arrow heads). **(C-E)** Cross sections at the level of the midbrain of whole mount *in situ* hybridizations of **(C)** *Lgals-1 L2* (inset is photographed from more anterior section), **(D)** *Lgals-1 L3*, and **(E)** *VE-cadherin*. Expression of both *Lgals-1 L2* and *L3* is observed in blood vessels in the brain (arrowhead in C and D) and in the retinal vessels (arrow in C and D) and colocalizes with the expression of EC marker *VE-cadherin*.

Figure 3. Loss of zebrafish galectin-1 L2 and L3 results in hemorrhages in the brain and defective vessel formation.

(A-D) o-Dianisidine staining for hemoglobin on 2.5 dpf embryos. **(A)** wild type control or injected with **(B)** *Lgals1 L2* AT-MO, **(C)** *Lgals-1 L3* ATG-MO, **(D)** both *Lgals-1 L2* and *L3* ATG-MOs. Co-injection of *L2* and *L3* ATG-MO results in severe hemorrhaging in the brain region (arrowheads). Arrow in **(A)** shows blood accumulating on the yolk and in the heart of a control embryo. **(E)** Schematic drawing of blood vessels in the dorsal brain at 2.5 dpf (modified from (46)). **(F-H)** Projection of Z-stacks made by confocal microscopy from *Tg(fli1:egfp)*^{y1} transgenic embryos at the level of the dorsal brain vessels at 2.5 dpf. **(F)** wild type control embryo. **(G)** Embryos co-injected with *Lgals-1 L2* and -*L3* ATG-MO display aberrant sprouting and misguidance of the middle cerebral vein (MCeV) into the dorsal longitudinal vein (DLV) (arrowheads). Defective angiogenic sprouting is also observed in the mesencephalic vein (arrow). **(H)** Co-injection of the *Lgals-1 L2* and *L3* splice-MO shows similar defects in angiogenic

sprouting of the brain vessels. DLV, dorsal longitudinal vein; MCeV, middle cerebral vein; MsV mesencephalic vein; MtA, metencephalic artery; PCeV, posterior cerebral vein.

Figure 4. Hampered tumor growth and lack of responsiveness to anginex in galectin-1 deficient mice.

(A) F9 teratocarcinoma tumor growth in gal-$1^{+/+}$ (solid squares) and gal-$1^{-/-}$ (solid triangles) mice. #$p<0.001$. **(B)** Immunohistochemical evaluation of vasculature and gal-1 expression in tumors from gal-$1^{+/+}$ (upper panels) and gal-$1^{-/-}$ (lower panels) mice. The left panels show vessel staining with EC marker 9F1 (brown). In the right panel, gal-1 staining (brown) is shown in consecutive sections. Bars represents 20 μm. **(C)** Quantification of microvessel density (MVD) in tumors from gal-$1^{+/+}$ (black bars) and gal-$1^{-/-}$ (white bars) mice. *$p<0.001$ vs. wild type mice. **(D)** F9 teratocarcinoma tumor growth in gal-$1^{+/+}$ mice during treatment with PBS (solid squares) or anginex (open squares). #$p<0.001$ vs. control. **(E)** Quantification of microvessel density (MVD) in gal-$1^{+/+}$ mice after treatment with PBS or anginex. *$p<0.05$ vs. untreated. **(F)** F9 teratocarcinoma tumor growth in gal-$1^{-/-}$ during treatment with PBS (filled triangles) or anginex (open triangles). ns=non significant.

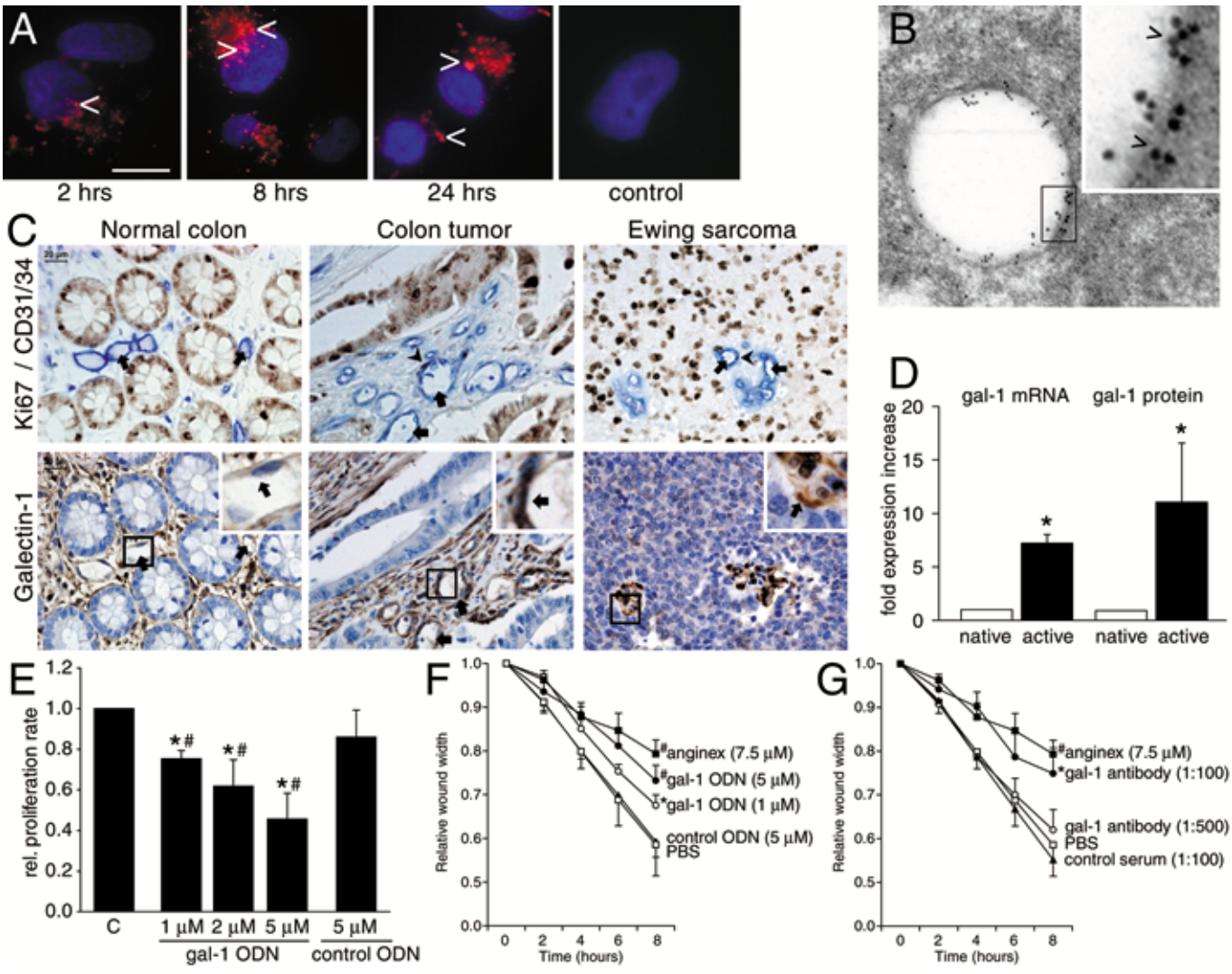
A
2 hrs
8 hrs
24 hrs
control
B
C
Normal colon
Colon tumor
Ewing sarcoma
Ki67 / CD31/34
Galectin-1
D
gal-1 mRNA
gal-1 protein
fold expression increase
native
active
native
active
E
rel. proliferation rate
C
1 µM
2 µM
5 µM
5 µM
gal-1 ODN
control ODN
F
Relative wound width
Time (hours)
#anginex (7.5 µM)
#gal-1 ODN (5 µM)
*gal-1 ODN (1 µM)
control ODN (5 µM)
PBS
G
Relative wound width
Time (hours)
#anginex (7.5 µM)
*gal-1 antibody (1:100)
gal-1 antibody (1:500)
PBS
control serum (1:100)

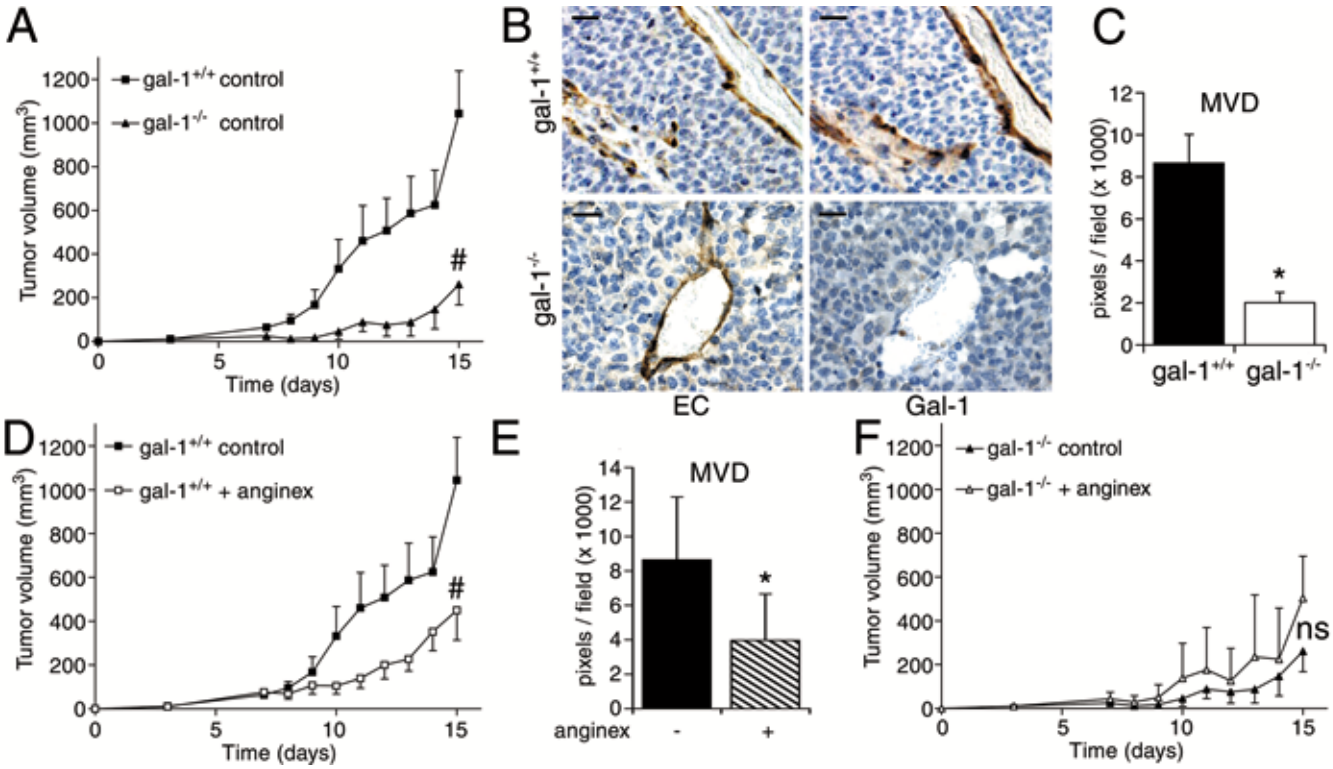
A
gal-1+/+ control
gal-1-/- control
Tumor volume (mm3)
Time (days)
#
B
gal-1+/+
gal-1-/-
EC
Gal-1
C
MVD
pixels / field (x 1000)
gal-1+/+
gal-1-/-
*
D
gal-1+/+ control
gal-1+/+ + anginex
Tumor volume (mm3)
Time (days)
#
E
MVD
pixels / field (x 1000)
anginex
-
+
*
F
gal-1-/- control
gal-1-/- + anginex
Tumor volume (mm3)
Time (days)
ns

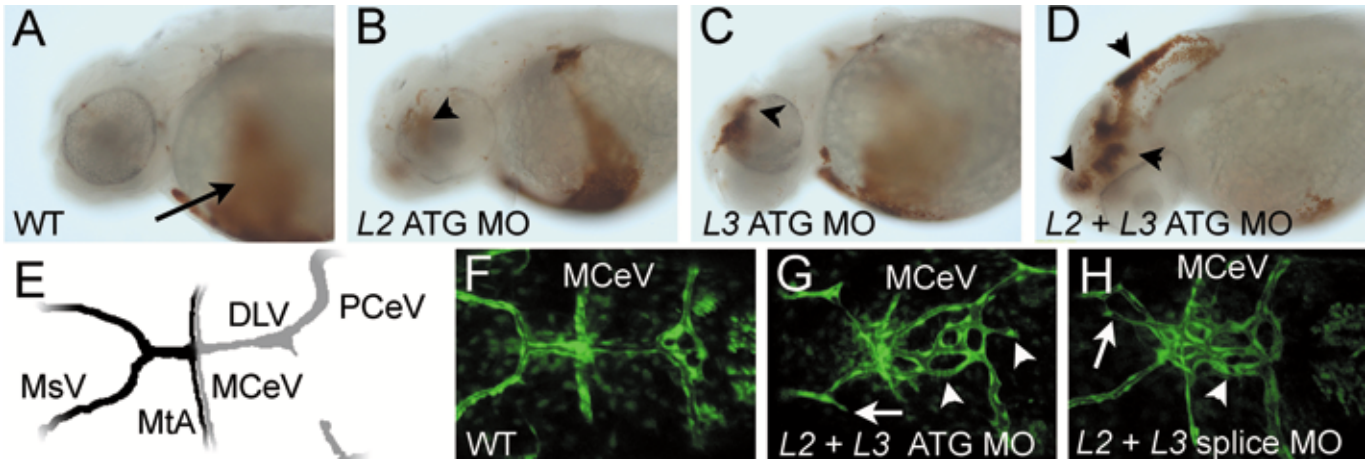
A
WT
B
L2 ATG MO
C
L3 ATG MO
D
L2 + L3 ATG MO
E
DLV
PCeV
MsV
MCeV
MtA
F
MCeV
WT
G
MCeV
L2 + L3 ATG MO
H
MCeV
L2 + L3 splice MO

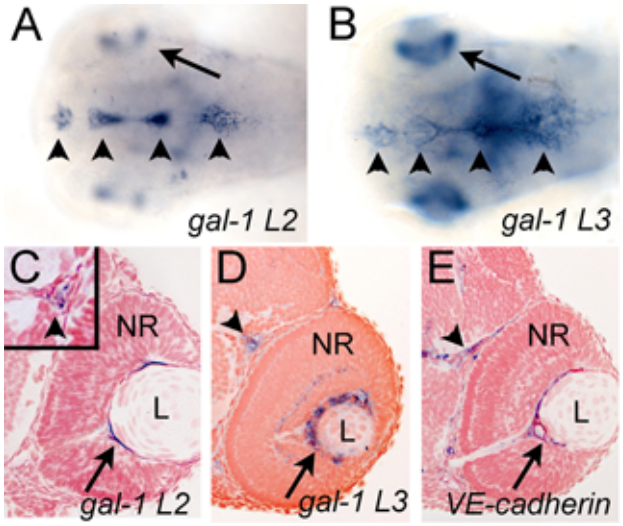
A
gal-1 L2
B
gal-1 L3
C
NR
L
gal-1 L2
D
NR
L
gal-1 L3
E
NR
L
VE-cadherin

Supplementary data

Results

Multiple screens against cDNA libraries of activated EC identified galectin-1 (gal-1) as the receptor for anginex **(Suppl. Table 1)**. Galectin-1 was found most frequently (15%) while no other members of the galectin family were identified. The identification of fibronectin, of which a previous study reported that it facilitates transport of anginex to the tumor vasculature (1), confirmed the validity of the approach.

The interaction was confirmed using three approaches i) Double staining of anginex treated EC showed co-localization of anginex and gal-1 **(Suppl. Fig. 1A)**. ii) Analysis of NMR spectra revealed chemical shift changes of certain resonances from gal-1 upon addition of anginex, indicative of a specific molecular interaction **(Suppl. Fig. 1B)**. iii) Plasmon resonance spectroscopy (BIAcore analysis) was used to further define the kinetics and stoichiometry of the interaction. To that end, gal-1 was immobilized on a BIAcore sensor chip which was verified with a rabbit polyclonal anti-gal-1 antibody **(Suppl. Fig. 1C)**. Addition of anginex resulted in a concentration dependent change in resonance response units **(Suppl. Fig. 1D)**. Analysis of the binding kinetics revealed a 1:1 Langmuir association with a rate constant (ka) of ~6.5x103 Ms-1, while the dissociation kinetics followed a biphasic pattern with dissociation rate constants of 4.2x10-2 s-1 and 5.9x10-4 s-1, respectively **(Suppl. Fig. 1E)**.

The *in vivo* role of gal-1 in angiogenesis was studied in the chick chorioallantoic membrane (CAM). Treatment of the CAM with a rabbit polyclonal anti-gal-1 antibody induced a significant inhibition of microvessel density, similar as previously published for anginex albeit less pronounced **(Suppl. Fig. 2A)**. Interestingly, treatment caused tortuous and irregular growth of the vessels, suggesting a defect in vascular guidance **(Suppl. Fig. 2B)**.

In the tumors of gal-1 null mice, several parameters of vessel architecture were decreased, indicative of a less comples and less developed vasculature **(Suppl. Table 2)**. Galectin-1 has been shown to mediate apoptosis in activated T cells, which could also contribute positively to tumor growth (2). To determine whether this also occurred in our tumor model we quantified the amount of peripheral blood leukocytes and the presence of CD45+ and CD8+ cells in the tumors. In our teratocarcinoma model there was no significant difference in these parameters between gal-1+/+ and gal-1-/- animals **(Suppl. Fig. 3)** which strongly suggests that, in this model, impaired tumor progression in gal-1 null mice largely results from decreased angiogenesis.

In addition, anginex treatment did not significantly affect the number of infiltrating CD45+ or CD8+ cells in the tumors of both the wild type and null mice **(Suppl. Fig. 4)**.

Materials and Methods

Yeast two-hybrid screening

Yeast two-hybrid screening was performed using the MATCHMAKER GAL4 Two-Hybrid System 3 (Clontech) according to the manufacturers instructions. In short, the artificial anginex gene (3) was PCR amplified and cloned into bait vector pGBKT7 in frame with the GAL4 DNA binding domain (pBD-Ax). The construct was tested for absence of transcriptional activation and toxicity. Subsequently, yeast *AH109* cells were co-transformed with pBD-Ax, *Sma*I-linearized prey vector (pGADT7), and a cDNA library which was generated from activated HUVEC mRNA. Following growth on media plates selective for reporter gene activation, prey plasmids from positive yeast colonies were isolated using CHROMA SPIN-1000 columns (Clontech), shuttled into *E.Coli*, and sequenced using an

automatic DNA-sequencer (AbiPrism377, Applied Biosystems). Confirmation of interaction was performed by targeted transformation of the specific constructs using the small-scale yeast transformation protocol as described in the yeast protocol handbook (Clontech).

Surface Plasmon Resonance

Real-time monitoring of molecular interactions was performed at 25°C using the BIAcore 1000 biosensor system (BiaCore) according to the manufacturer's instructions. In short, recombinant human galectin-1 (4) was immobilized to a CM5 sensor chip (BiaCore) via primary amine groups using the Amine Coupling Kit (BiaCore). For interaction analysis, 20 µl sample was diluted to various concentrations in HBS-EP (Biacore) and was injected using the KINJECT command at a flow rate of 30 µl/minute after which the flow cells were regenerated by injection of 20 µl regeneration buffer (10 mM glycine-HCl, pH 2.0). Association-rate (k_a) and dissociation-rate (k_d) constants were obtained by analysis of the sensograms using the Biaevaluation software, version 3.2. All measurements were performed at least in duplicate at all concentrations and the experiment was performed in duplo.

NMR Spectroscopy

For NMR measurements, 5 mg of recombinant human galectin-1 (4) was dissolved in 600 µl of 10mM potassium phosphate buffer made with 95%/5% H_2O/D_2O at pH 5.2. Freeze-dried anginex was dissolved in 10 µl of the same buffer and added to the galectin sample at the molar ratio of 1:2 (anginex:galectin). 2D-homonuclear TOCSY spectra (5) with WATERGATE for water suppression, were acquired on a Varian UNITY Plus-600 NMR spectrometer at 30°C. 2048 complex data points along t2 and 256 increments along t1 dimensions over a spectral width of 9000 Hz, were collected. A mixing time of 50 ms was used. Data were processed using a Gaussian window function and the program NMRPipe (6).

Electron Microscopy

For electron microscopy, HUVEC were grown on gelatin coated and glutaraldehyde fixed thermanox cover slips in normal HUVEC culture medium supplemented with 75 µM anginex. Subsequently, cells were fixed with 1% paraformaldehyde, and localization of anginex by jet freezing and freeze substitution was performed as described previously (7), using polyclonal rabbit anti-anginex antibody in combination with immunogold labeled goat anti-rabbit antibody (Aurion).

References

1. Akerman, M. E., Pilch, J., Peters, D. & Ruoslahti, E. (2005) *Proc Natl Acad Sci U S A* **102,** 2040-5.
2. Rubinstein, N., Alvarez, M., Zwirner, N. W., Toscano, M. A., Ilarregui, J. M., Bravo, A., Mordoh, J., Fainboim, L., Podhajcer, O. L. & Rabinovich, G. A. (2004) *Cancer Cell* **5,** 241-51.
3. Brandwijk, R. J., Nesmelova, I., Dings, R. P., Mayo, K. H., Thijssen, V. L. & Griffioen, A. W. (2005) *Biochem Biophys Res Commun* **333,** 1261-1268.
4. Pace, K. E., Hahn, H. P. & Baum, L. G. (2003) *Methods Enzymol* **363,** 499-518.
5. Cavanagh, J. & Rance, M. (1992) *Journal of Magnetic Resonance* **96,** 670-678.
6. Delaglio, F., Grzesiek, S., Vuister, G. W., Zhu, G., Pfeifer, J. & Bax, A. (1995) *J Biomol NMR* **6,** 277-93.
7. Stuart, M. C., Damoiseaux, J. G., Frederik, P. M., Arends, J. W. & Reutelingsperger, C. P. (1998) *Eur J Cell Biol* **76,** 77-83.
8. Wild, R., Ramakrishnan, S., Sedgewick, J. & Griffioen, A. W. (2000) *Microvasc Res* **59,** 368-76.

Supplementary Table 1. Results of yeast two-hybrid screening with anginex as bait.

Clone name	number of clones
Galectin-1	9
Methallothionein 2A	3
Fibronectin (partial)	3
Pecanex-like3	3
Keratin	2
Filamin A	1
GCN1	1
Methyltransferase	1
False positives[a]	23
Undetermined[b]	14
Total	60

[a] Failed to show interaction following repeated plating or high selection plates or in targeted yeast transformation (see Materials & Methods)**.**

[b] Clones of which the interaction has not been confirmed or that have not been identified by sequencing.

Supplementary Table 2. Vascular parameters in F9 tumors of wild type and mutant mice.

Mice	Vessel Density[a]	End Points[b]	Branch Points[c]	Vessel Length[d]
gal-1$^{+/+}$	8642 ± 666	147 ± 11	10 ± 1.1	11.6 ± 1.0
gal-1$^{-/-}$	2009 ± 269$^{\#}$	48.8 ± 3.4$^{\#}$	2.0 ± 0.6$^{\#}$	2.8 ± 0.3$^{\#}$

On the last day of the experiment, tumors were excised. Tumors without apparent widespread necrosis were embedded in tissue freezing medium (Miles Inc.) and snap frozen in liquid nitrogen. Preparation and procedures were done as described earlier(8).

[a] After binarization of the images from CD31-staining, microvessel density was estimated by scoring the total number of white pixels per field.

[b] Mean number of vessel end points as determined after skeletonization of the images(8).

[c] Mean number of vessel branch points/nodes per image.

[d] Mean total vessel length per image.

All results are expressed as mean pixel counts per image ± standard error from 20 images.

# $p<0.05$ vs. wildtype.

Supplementary figure legends

Supplementary Figure 1. Confirmation and characterization of the interaction between galectin-1 and anginex.

(A) Fluorescence double staining of anginex (red) and galectin-1 (green) in anginex treated EC. Co-localization (yellow) is indicated with arrow heads. Nuclei are counterstained with DAPI. Bar in the left panel represents 10 µm **(B)** NMR analysis of the galectin-1/anginex interaction. The Hα - NH fingerprint region is shown from 2D TOCSY spectra of pure galectin-1 (red) and of galectin-1 to which anginex was added (blue) at a molar ratio of 1:2 (anginex:galectin-1). Single color signals and incomplete overlapping color signals indicate a shift in resonances upon addition of anginex and are indicative of galectin-1/anginex interactions. **(C)** Validation of galectin-1 immobilization on a BIAcore sensor chip and of protein preservation with galectin-1 antibody (n=2). Following immobilization of galectin-1, increasing amounts of rabbit polyclonal anti-galectin-1 antibody were run over the chip. As negative control, rabbit polyclonal anti-anginex antibody was used. **(D)** Surface plasmon resonance analysis of interaction between anginex and galectin-1 (n=3). Increasing amounts of anginex were run over the chip with immobilized galectin-1, resulting in an increase in response units (RU). **(E)** Analysis of binding kinetics of interaction between anginex and immobilized galectin-1. The upper panel shows a representative dose response sensogram for anginex. The areas used for model fitting are shown in bold while the residual plot in the middle panel shows minimal discrepancies between the experimental data and the fit. In the lower panel the observed association rates (k_{obs}) are plotted as a function of analyte concentration with a slope equal to the association rate constant (k_a).

Supplementary Figure 2. Altered vessel numbers and morphology in chorioallantoic membranes after treatment with galectin-1 protein and antibody.

(A) Quantification of microvessel density in the CAMs after treatment with different dilutions of anti-galectin-1 antibody. *$p<0.05$ vs. control. **(B)** Representative images of CAMs after treatment with PBS (control) and anti-galectin-1 antibody. Note the tortuous and irregular growth of the vessels in the latter.

Supplementary Figure 3. The number of circulating leukocytes and tumor infiltrating leukocytes is unaltered in galectin-1 mutant mice.

(A) Immunohistochemical evaluation of tumor infiltrating leukocytes in galectin-$1^{+/+}$ (upper panels) and galectin-$1^{-/-}$ (lower panels) mice. The left panels show $CD45^+$ cells (brown staining). In the right panel, $CD8^+$ cells are shown. **(B)** Quantification of $CD45^+$ and $CD8^+$ cells in tumors from galectin-$1^{+/+}$ (black bars) and galectin-$1^{-/-}$ (white bars) mice. **(C)** Quantification of total number of leukocytes in galectin-$1^{+/+}$ (black bars) and galectin-$1^{-/-}$ (white bars) mice.

Supplementary Figure 4. Anginex treatment does not affect leukocyte infiltration in galectin-1 wild type and mutant mice.

(A) Immunohistochemical evaluation of infiltrate in untreated tumors from galectin-$1^{+/+}$ (left panels) and in anginex treated tumors from galectin-$1^{+/+}$ (middle panels) and galectin-$1^{-/-}$ (right panels) mice. The upper panels show $CD8^+$ cells (brown staining). In the lower panels, $CD45^+$ cells are shown. **(B)** Quantification of $CD45^+$ and $CD8^+$ cells in untreated tumors from galectin-$1^{+/+}$ (black bars) and galectin-$1^{-/-}$ (white bars) as well as in anginex treated tumors from galectin-$1^{+/+}$ (downward diagonal) and galectin-$1^{-/-}$ (upward diagonal) mice.

Supplementary figure 1

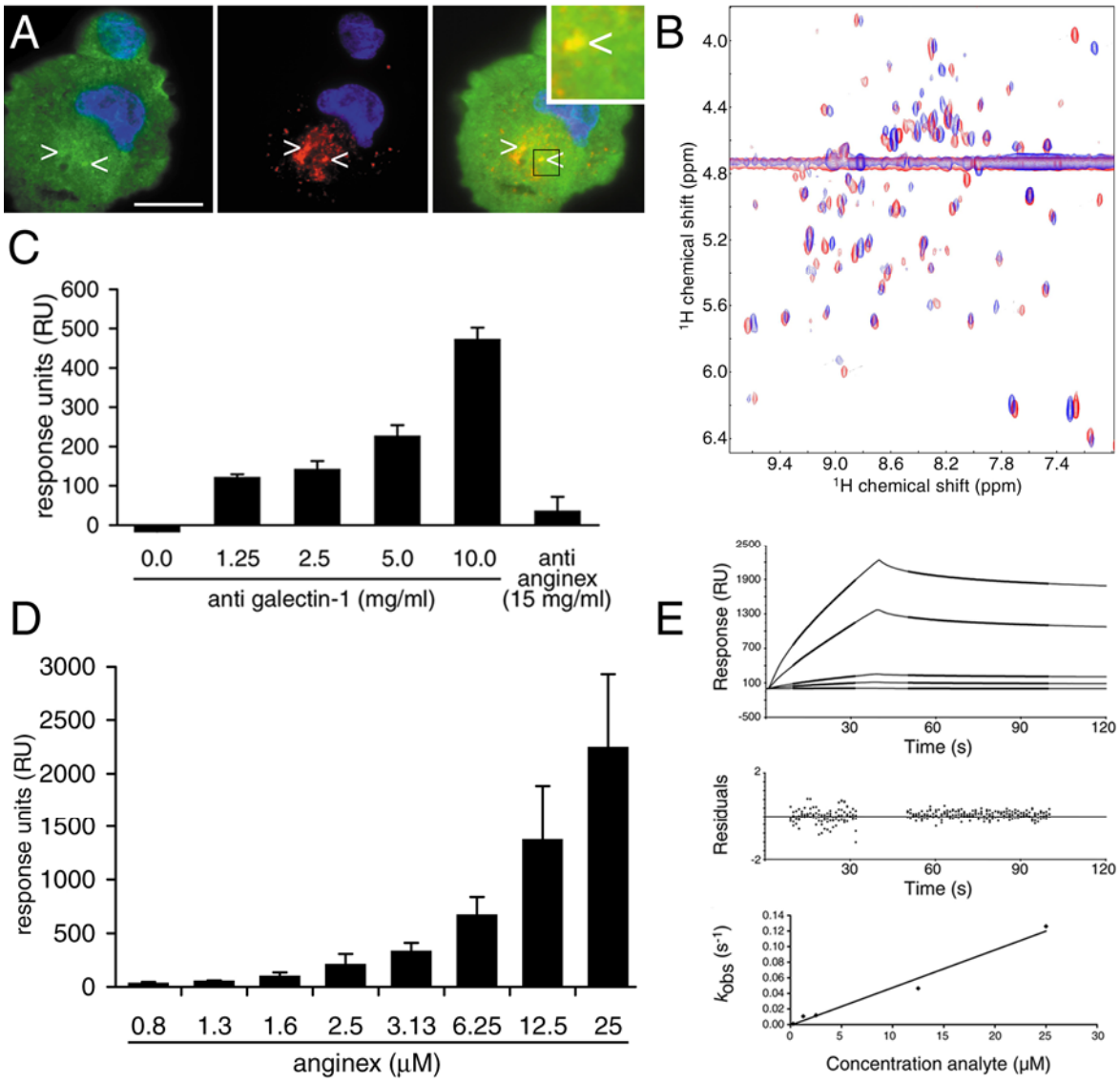

Supplementary figure 2

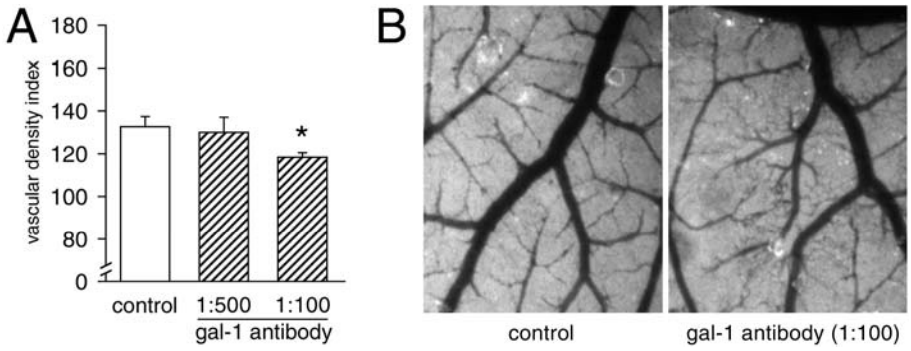

Supplementary figure 3

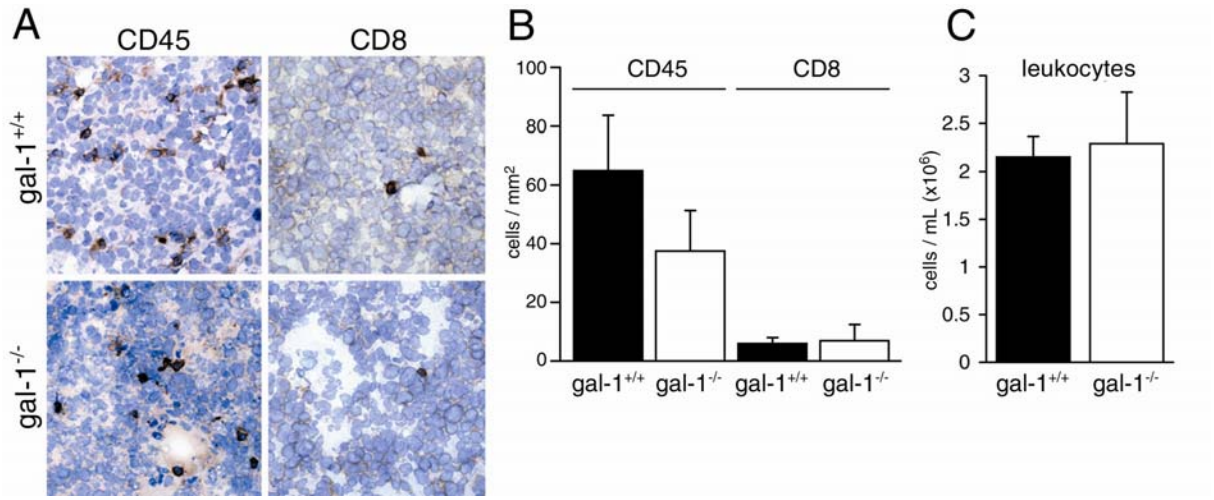

Supplementary figure 4